

Double pulse laser-induced breakdown spectroscopy of bulk aqueous solutions at oceanic pressures: interrelationship of gate delay, pulse energies, interpulse delay, and pressure

Anna P. M. Michel^{1,2,3,*} and Alan D. Chave¹

¹Department of Applied Ocean Physics and Engineering, Woods Hole Oceanographic Institution, Mail Stop 7, 266 Woods Hole Road, Woods Hole, Massachusetts 02543, USA

²Department of Mechanical Engineering, Massachusetts Institute of Technology, 77 Massachusetts Avenue, Cambridge, Massachusetts 02139, USA

³Currently at the Center for Mid-InfraRed Technologies for Health and the Environment, Princeton Institute for the Science and Technology of Materials, Princeton University, 70 Prospect Avenue, Princeton, New Jersey 08540, USA

*Corresponding author: apmichel@princeton.edu

Received 31 March 2008; accepted 6 June 2008;
posted 4 August 2008 (Doc. ID 94502); published 19 September 2008

Laser-induced breakdown spectroscopy (LIBS) has been identified as an analytical chemistry technique suitable for field use. We use double pulse LIBS to detect five analytes (sodium, manganese, calcium, magnesium, and potassium) that are of key importance in understanding the chemistry of deep ocean hydrothermal vent fluids as well as mixtures of vent fluids and seawater. The high pressure aqueous environment of the deep ocean is simulated in the laboratory, and the key double pulse experimental parameters (laser pulse energies, gate delay time, and interpulse delay time) are studied at pressures up to 2.76×10^7 Pa. Each element is found to have a unique optimal set of parameters for detection. For all pressures and energies, a short (≤ 100 ns) gate delay is necessary. As pressure increases, a shorter interpulse delay is needed and the double pulse conditions effectively become single pulse for both the 1.38×10^7 Pa and the 2.76×10^7 Pa conditions tested. Calibration curves reveal the limits of detection of the elements (5000 ppm Mg, 500 ppm K, 500 ppm Ca, 1000 ppm Mn, and 50 ppm Na) in aqueous solutions at 2.76×10^7 Pa for the experimental setup used. When compared to our previous single pulse LIBS work for Ca, Mn, and Na, the use of double pulse LIBS for analyte detection in high pressure aqueous solutions did not improve the limits of detection. © 2008 Optical Society of America

OCIS codes: 140.3440, 140.0140, 010.4450, 300.0300, 300.6365.

1. Introduction

Laser-induced breakdown spectroscopy (LIBS) has recently been identified as a laboratory analytical chemistry technique that is also suitable for use on environmental and geochemical samples in the field [1]. For example, several groups are evaluating the use of LIBS for space exploration [2–7]. Another en-

vironmental area in which there is a critical need for new chemical sensors is the ocean. Sensor development for use with underwater vehicles is ongoing, and a requirement is emerging for sensors suitable for deployment on permanent ocean observatories. One environment identified as potentially benefiting from application of an oceanic LIBS sensor is deep-sea hydrothermal vents. These features occur at mid-ocean ridges where seawater circulates through the permeable ocean crust, allowing the fluid to interact with the surrounding rock, resulting

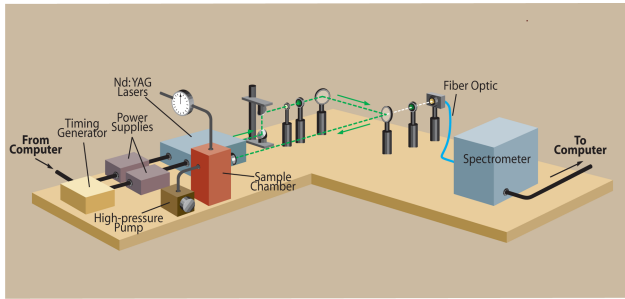


Fig. 1. (Color online) Laboratory setup for aqueous DP-LIBS experiments.

in major fluid chemical changes. At vent orifices, exit temperatures reach 200–405°C at ambient pressures from 8.1×10^6 to 3.6×10^7 Pa, corresponding to ocean depths of 800–3600 m [8].

At hydrothermal vents, as the hot fluids mix with seawater, further rapid chemical change occurs and some compounds precipitate out [9]. *In situ* chemical measurement of vent fluids is difficult due to their corrosive nature and high temperature. Collection of the fluid for analysis shipboard or in a terrestrial laboratory introduces irreversible chemical changes as the temperature and pressure of the fluid are altered during sample recovery.

Critical elements at hydrothermal vents include sodium, calcium, manganese, magnesium, and potassium. Sodium is the dominant cation in vent fluids, and its measurement provides insight into phase separation processes [10]. Calcium is the second most dominant cation in vent fluids and is typically found at a greater concentration in vent fluids

than in seawater [11]. Ca is released into vent fluids when Na is taken up in albitization reactions with the host rock [11]. Manganese exists as a trace metal in seawater but has a higher concentration in vent fluids due to leaching from the host rock [10]. Magnesium is practically nonexistent in hydrothermal vent fluids; however, if any is detected in vent fluids, contamination by entrainment of ambient seawater is indicated [10]. Potassium is typically highly enriched in vent fluids due to leaching from basalts [10]. In vent fluids, concentrations range from approximately 250 ppm to 23,163 ppm for Na, 0.6 ppm to 399 ppm for Mn, 0 ppm to 4477 ppm for Ca, 0 ppm to 3166 ppm for K, and 0 ppm for Mg [8]. In seawater, concentrations are approximately 10,933 ppm Na, <0.001 ppm Mn, 419 ppm Ca, 405 ppm K, and 1300 ppm Mg [8].

Development of an oceanic LIBS sensor necessitates laboratory investigations into the system parameters for the detection of analytes under high pressure bulk aqueous conditions. Although LIBS analysis on liquids is more difficult than for solid or gaseous samples, a few studies have focused on dissolved analytes in bulk solutions [12–19]. The inherent difficulty of performing LIBS analysis of aqueous solutions is a result of reduction in plasma light intensity and emission lifetime from quenching by the liquid, spectral line broadening due to the Stark effect, and moving breakdown that causes fluctuations in the distance between the plasma and the collection fiber optic [12,13,20–22]. The breakdown threshold in aqueous solutions is also significantly greater than for solids [23]. Laser-induced plasmas

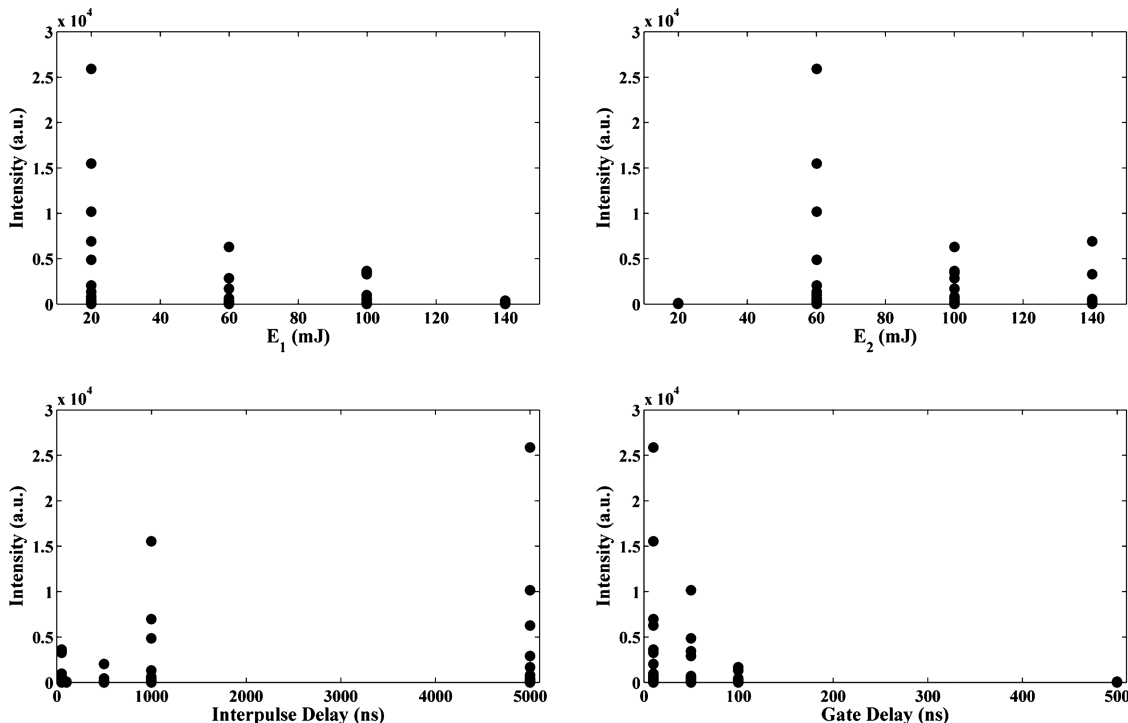


Fig. 2. Mg (I) (518.4 nm peak) optimization at 1×10^5 Pa. Each dot represents the peak intensity measured at one condition.

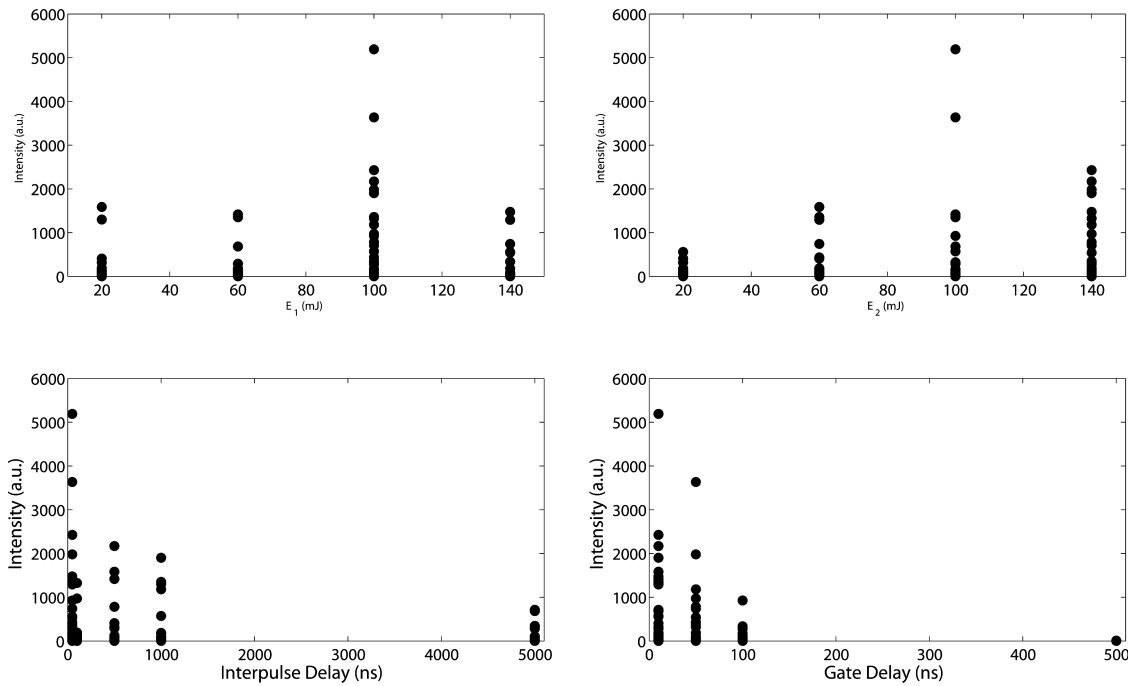


Fig. 3. Mg (I) (518.4 nm peak) optimization at 1.38×10^7 Pa. Each dot represents the peak intensity measured at one condition.

are weak in water, as they are cooled by bremsstrahlung and shockwave emissions and by thermal conduction. The rapid cooling of plasmas formed in aqueous solutions at atmospheric pressure also increases electron-ion recombination, causing plasma emission to last of the order of a few microseconds [24].

In 1984, Cremers *et al.* showed that several elements, including Na, K, Mg, and Ca, could be iden-

tified in bulk aqueous solution using double pulse (DP) LIBS. This work, carried out at atmospheric pressure, showed that DP-LIBS improved the detection limit for metals and ions in bulk aqueous solution [12]. In DP-LIBS of aqueous solutions, the first laser pulse causes the formation of a laser-induced cavitation bubble. The second laser pulse produces a plasma within this bubble [24,25]. This is in contrast to single pulse (SP) LIBS, where the plasma

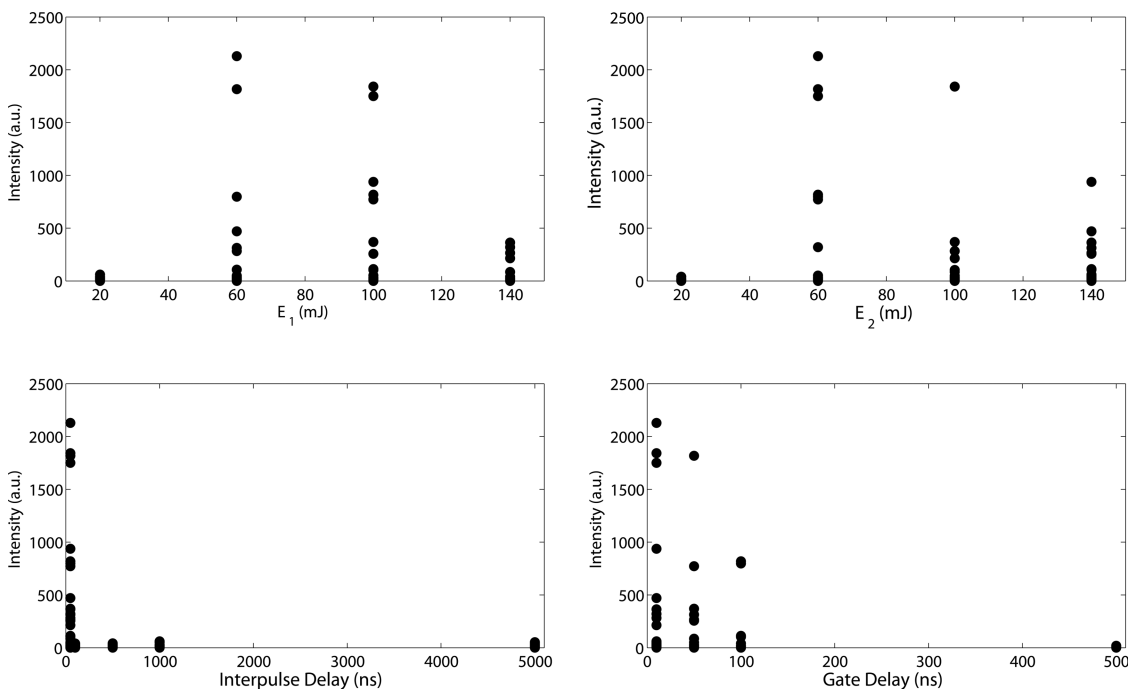


Fig. 4. Mg (I) (518.4 nm peak) optimization at 2.76×10^7 Pa. Each dot represents the peak intensity measured at one condition.

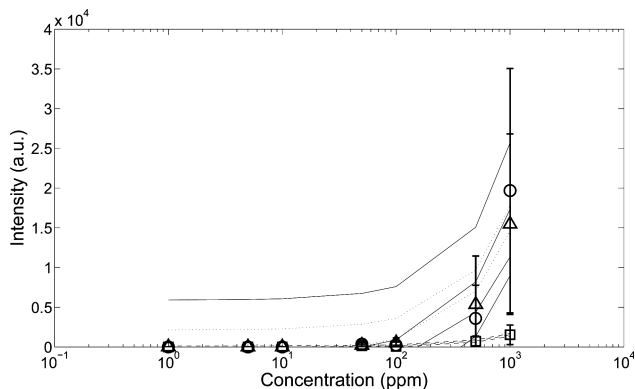


Fig. 5. Calibration curves calculated by a linear least squares fit of the concentration data and their 95% confidence limits on the coefficients for the Mg (I) 518.4 nm peak, \circ , solid line = 1×10^5 Pa; \square , dashed line = 1.38×10^7 Pa; Δ , dotted line = 2.76×10^7 Pa ($E_1 = 60$ mJ, $E_2 = 60$ mJ, $t_d = 50$ ns, and $\Delta T = 50$ ns).

is simply formed in a liquid environment. In DP-LIBS, the duration of the laser-induced plasma in the bubble is of the order of a few microseconds while the bubble lifetime is of the order of a few hundred microseconds. Therefore, it can be assumed that the plasma from the second pulse is expanding in a quasi-stationary environment induced by the first laser pulse [25,26]. When the bubble is first formed, its pressure is greater than that of the surrounding liquid and the bubble begins to expand, leading to a pressure drop. At the point of maximum expansion, the bubble pressure is less than the pressure of the surrounding fluid and the bubble begins to collapse. During this collapsing phase, the temperature and pressure in the bubble again increase. If there is enough energy stored within the bubble, reexpansion can take place; furthermore, many oscillations of expansion and compression are possible [24]. By adjusting the interpulse delay (ΔT , the time between the firing of laser pulse one and laser pulse two) between the laser pulses, it is possible to select the phase that the bubble is in such that bubble pressure

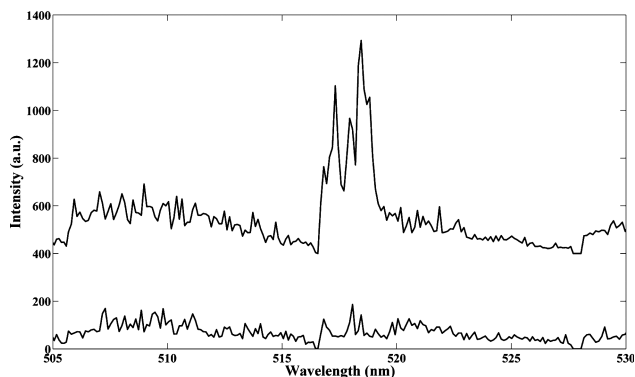


Fig. 6. Spectra of the Mg (I) peak (518.4 nm) at 2.76×10^7 Pa. The concentrations from bottom to top are 1000 ppm and 5000 ppm. ($E_1 = 60$ mJ, $E_2 = 60$ mJ, $t_d = 50$ ns, and $\Delta T = 50$ ns). For clarity, the spectra have been offset from each other by 500 a.u.

is at a nadir. However, if ΔT is too long or too short, the plasma will expand in a high pressure environment, causing the spectral lines to be broadened due to collisions [24]. Selection of the delay time between the first and the second pulses is therefore critical for LIBS analysis of bulk liquids.

Since the pioneering work of Cremers *et al.*, several groups have used DP-LIBS for the detection of analytes in bulk liquids [12,14,18,26–28] and more recently for bulk solutions at high pressures [15,16]. In Michel *et al.* [15], analyte detection in high pressure bulk solutions was shown to be highly dependent on ΔT . When a shorter ΔT was used ($\ll 1 \mu\text{s}$), the signal intensity was enhanced compared to when longer ΔT were employed. However, it was noted that this time may not be long enough for cavitation bubbles to fully form and expand, as occurs at low pressure. Michel *et al.* also found that the optimal energy levels needed for emission varied by analyte [15]. Furthermore, Lawrence-Snyder *et al.* [16] reported that increasing solution pressure reduces double pulse emission enhancement, with little improvement noted over single pulse for solutions at pressures above 1×10^7 Pa.

In [19], optimization of SP conditions for three analytes (Na, Mn, and Ca) was reported; yet, the limits of detection were not at the levels that were expected to be achievable. Through optimization of DP experimental parameters, we aim to improve the limits of detection for the same three analytes and to establish the limits of detection for additional elements. Although Lawrence-Snyder *et al.* previously reported on the use of DP-LIBS at high pressures and found no enhancement of detectability above 1×10^7 Pa [16], several differences exist between these studies. Lawrence-Snyder *et al.* reported their findings using an orthogonal beam geometry (the collection of the plasma light is orthogonal to the path of the excitation laser beam, which would be impractical for an oceanic sensor in many applications), their work does not extend to the ambient pressures for most hydrothermal vents, and optimization of laser pulse energies was not carried out. In this paper, through a more comprehensive optimization, the use of DP-LIBS at pressures up to 2.76×10^7 Pa is investigated, and the limits of detection for five key elements are determined.

2. Experimental

Double pulse high pressure aqueous LIBS experiments were completed using the laboratory setup detailed in Fig. 1. Two Big Sky CFR-200 Nd:YAG lasers configured with the beams collinearly aligned prior to exiting the aperture were operated at 1064 nm with a 5 Hz repetition rate. Each laser is equipped with a motorized variable attenuator serially controlled by a computer, enabling the laser pulse energies (E_1 and E_2) to be varied independently from 0 mJ to 200 mJ in increments of approximately 1 mJ. Plasma emission is collected with an Echelle spectrometer (LLA Echelle ESA 3000) that covers

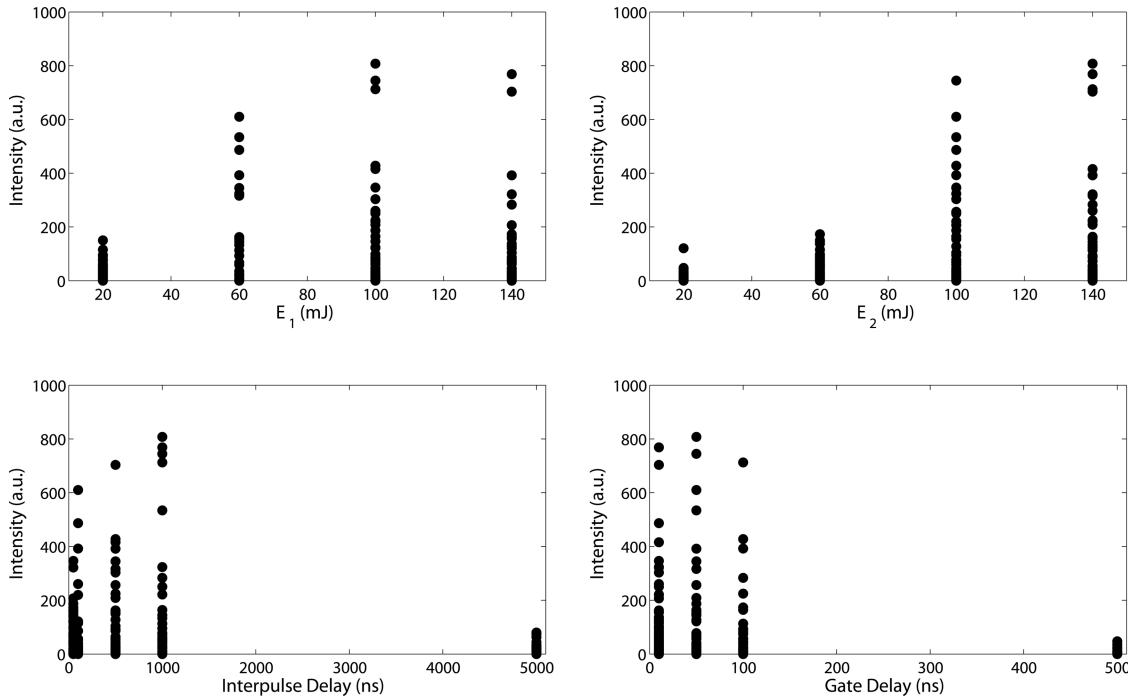


Fig. 7. K (I) (769.9 nm peak) optimization at 1×10^5 Pa. Each dot represents the peak intensity measured at one condition.

the spectral region from 200 to 780 nm with a resolution of 10–50 pm. Accurate timing of the firing of the lasers, ΔT , and the gate delay (t_d , the time between the firing of the second laser pulse and the turn-on of the spectrometer) is controlled by a timing box (Berkeley Nucleonics Corporation Model 565). The integration time of the spectrometer, gate width (t_b), is also controllable.

An $8.89 \text{ cm} \times 8.89 \text{ cm} \times 8.89 \text{ cm}$ titanium sample chamber that holds 27 ml of liquid connects to a high pressure metering pump (Eldex Model A-30-S) using Swagelok fittings to pressurize samples up to 4.1×10^7 Pa. The sample chamber is equipped with a sapphire window (Meller Optics, 2.54 cm diameter \times 0.64 cm thickness, antireflection coated at 532 nm/1064 nm, custom part) that allows laser pulses to

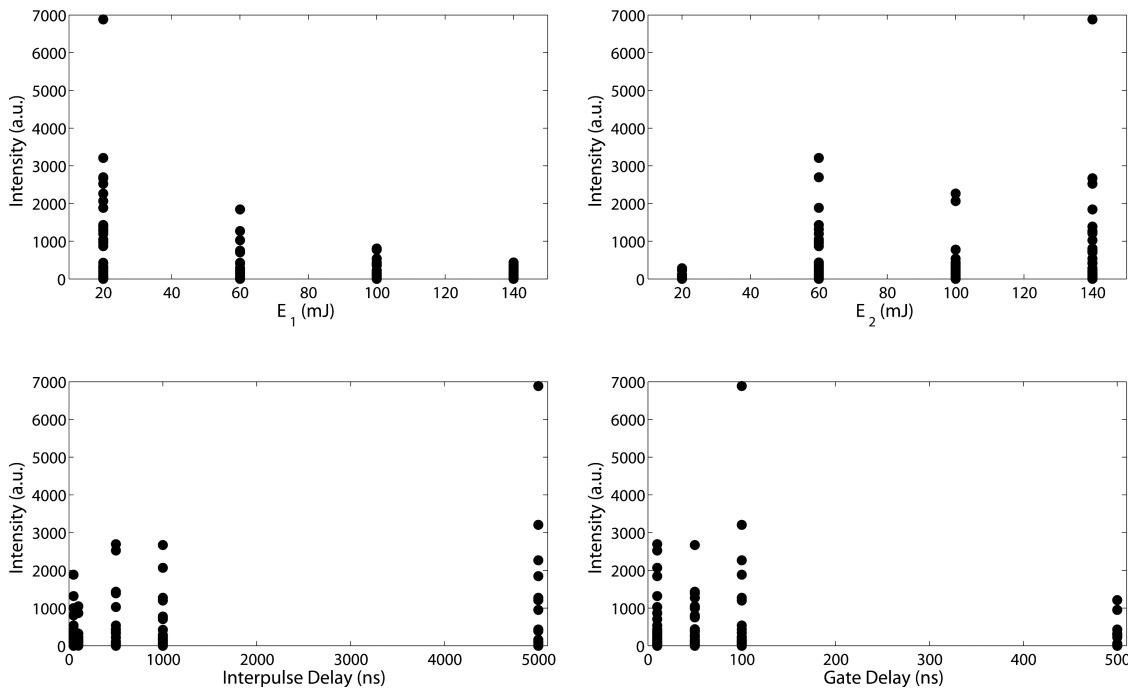


Fig. 8. K (I) (769.9 nm peak) optimization at 2.76×10^7 Pa. Each dot represents the peak intensity measured at one condition.

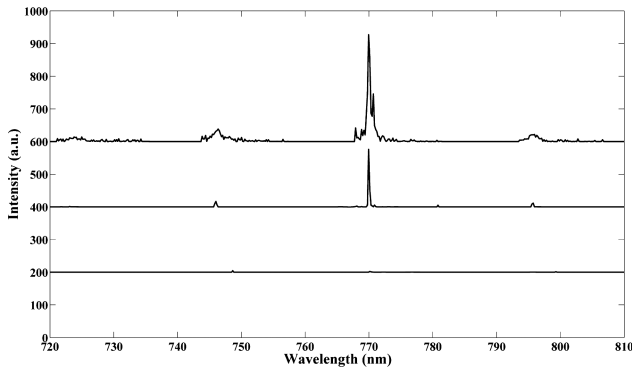


Fig. 9. Spectra of the 769.9 nm K (I) peak at 2.76×10^7 Pa. Concentrations of spectra from bottom to top are 100 ppm, 500 ppm, 1000 ppm. ($E_1 = 100$ mJ, $E_2 = 140$ mJ, $t_d = 1000$ ns, and $\Delta T = 50$ ns). For clarity, the spectra have been offset from each other by 200 a.u.

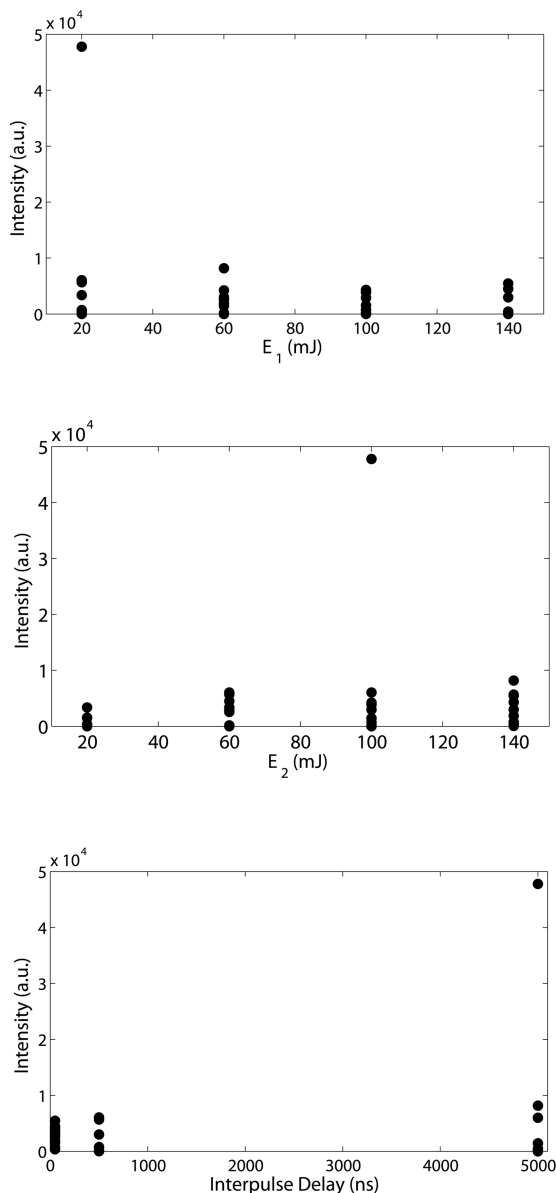


Fig. 10. Ca (I) (422 nm peak) optimization at 1×10^5 Pa. Each dot represents the peak intensity measured at one condition.

enter the sample chamber. A series of antireflection-coated optics are used to focus the laser pulses into the sample chamber and to focus the plasma light onto an optical fiber for delivery to the spectrometer. The plasma emission is collected collinear to the incoming laser beams to simulate the design that would be most practical for an ocean-going LIBS system. Data are collected using ESAWIN software. Laser pulse energy is measured using an energy meter (Coherent J25LP-MB and FieldMaxII-Top).

For DP-LIBS optimization studies, peak intensities for five analytes (Mg, K, Na, Ca, and Mn) were measured over a range of system parameters: E_1 , E_2 , t_d , and ΔT . E_1 and E_2 were each tested at 20, 60, 100, and 140 mJ. Average irradiance (I_f) at the beam waist for our setup can be estimated from

$$I_f = \frac{\pi E D^2}{4 \tau_L f^2 \lambda^2 M^4}, \quad (1)$$

where E is the laser pulse energy, D is the diameter of the illuminated aperture of the focusing lens (25 mm), τ_L is the pulse duration at the full peak width at half of the maximum intensity (FWHM, 7.5 ns), f is the focal length of the focusing lens (35 mm), λ is the laser wavelength (1064 nm), and M^2 is the beam propagation ratio, which is typically 2–10 for Nd:YAG lasers (we estimate a value of 6 for our setup) [29]. Using pulse energies of 20, 60, 100, and 140 mJ corresponds to irradiance at the beam waist of $\approx 2.62 \times 10^{12}$, 7.87×10^{12} , 1.31×10^{13} , and 1.84×10^{13} W/cm², respectively.

For comparisons of pressure effects on optimal experimental parameters, studies were conducted at three pressures, 1×10^5 , 1.38×10^7 , and 2.76×10^7 Pa, which correspond to ocean depths of approximately 0, 1362, and 2724 m, respectively. For Mg and K, t_d was tested at 10, 50, 100, and 500 ns, and ΔT was tested at 50, 100, 500, 1000, and 5000 ns. For Na, Ca, and Mn, t_d was held constant at 50 ns, and the ΔT was tested at 50, 500, and 5000 ns. Each combination of these conditions was evaluated for a total of 320 conditions for Mg and K and 48 conditions for Mn, Na, and Ca. For all studies, t_b was held constant at 200 ns and the amplification of the Echelle spectrometer was set to the maximum value of 4000.

Five spectra (10 spectra for calibration curves) were taken at each condition. All spectra were composed of 100 shot accumulations. To account for the high resolution of the spectrometer and the peak broadening that occurs from liquids, all the data were grouped into sets of nine wavelengths. Each set of data points (9×5 for the optimization or 9×10 for the calibration curves) was processed using extreme value statistics as described by Michel and Chave [30]. All the calibration curves were made at three pressures (1×10^5 , 1.38×10^7 , and 2.76×10^7 Pa). For each analyte, a linear least squares fit of the concentration data was computed in addition to 95% confidence limits on the

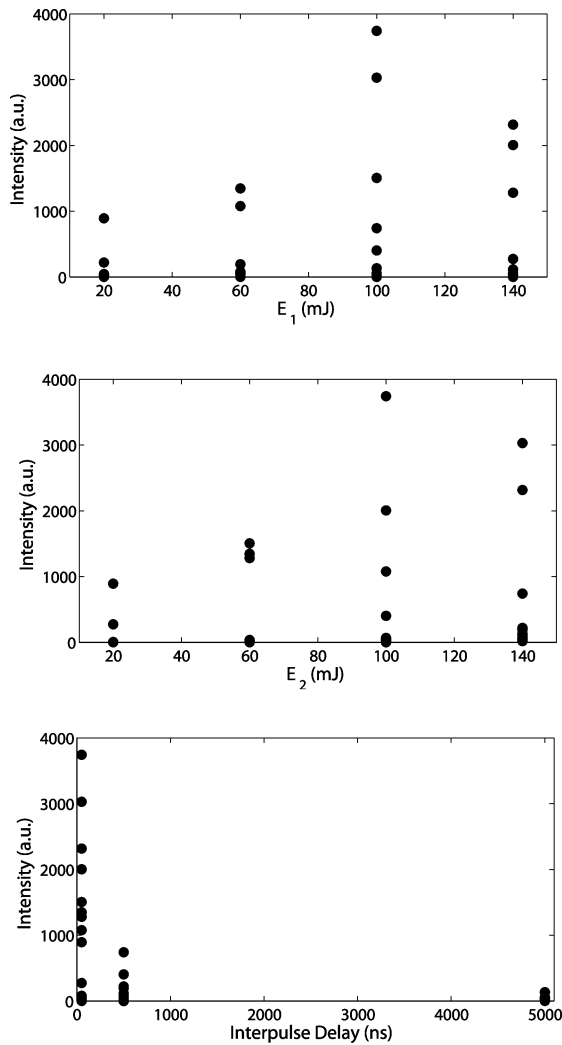


Fig. 11. Ca (I) (422 nm peak) optimization at 1.38×10^{17} Pa. Each dot represents the peak intensity measured at one condition.

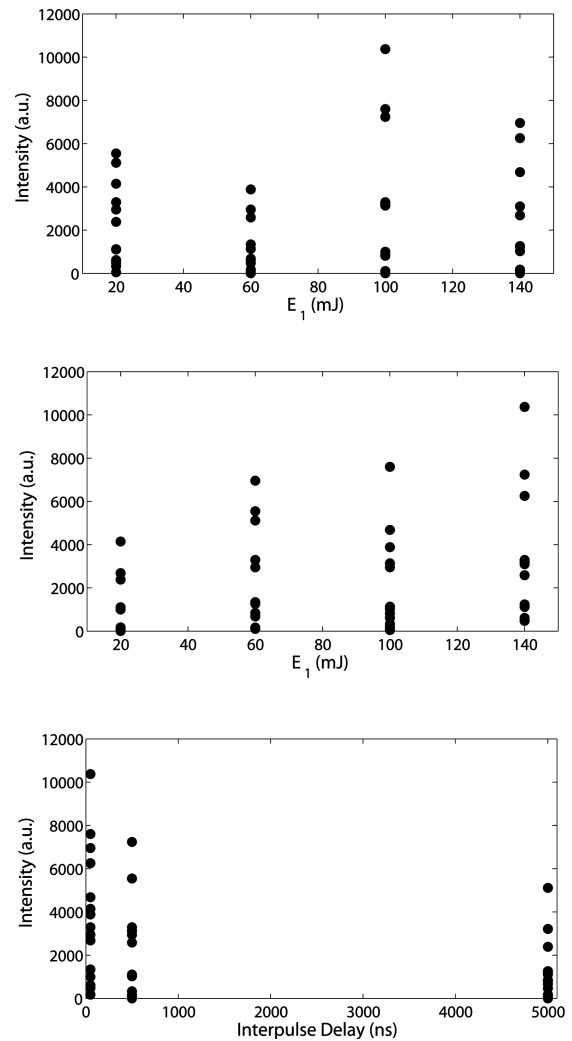


Fig. 12. Ca (I) (422 nm peak) optimization at 2.76×10^7 Pa. Each dot represents the peak intensity measured at one condition.

coefficients. Where shown, error bars represent the double-sided 95% confidence limits for the extreme value parameters defined in [30].

Solutions were made using $\text{MgCl}_2 \cdot 6\text{H}_2\text{O}$, NaCl, KCl, $\text{MnSO}_4 \cdot \text{H}_2\text{O}$, and $\text{CaCl}_2 \cdot \text{H}_2\text{O}$ dissolved in DI water. All concentrations are given in parts per million (ppm, wt./vol.). For the optimization studies, the concentrations used were 5000 ppm Mg, 1000 ppm K, 100 ppm Na, 1000 ppm Ca, and 1000 ppm Mn.

3. Results and Discussion

For DP-LIBS of high pressure aqueous solutions, optimizing the key parameters (E_1 , E_2 , t_d , and ΔT) individually for each element of interest is essential for identifying the conditions under which each can be detected. The optimization studies presented here show that these conditions are pressure dependent for DP-LIBS. Outside the range of these conditions, some of the elements prove to be undetectable with the present apparatus. Through optimization of the parameters, a set of conditions may be established

that allow calibration curves to be constructed to infer the limits of detection for high pressure bulk aqueous solutions.

A. Magnesium

Results for the 518.4 nm Mg (I) peak are presented in Figs. 2–4. From these figures, the need for a short t_d (≤ 100 ns) is evident, irrespective of solution pressure or laser pulse energy. At all solution pressures, when t_d reaches 500 ns, Mg (I) is no longer detectable. When the solution is at atmospheric pressure (1×10^5 Pa), the peak intensity recorded was greatest with use of a longer ΔT (1000–5000 ns) (Fig. 2). It was also advantageous to keep E_1 at a lower level than was used for E_2 . For example, two favorable conditions were $E_1 = 60$ mJ, $E_2 = 100$ mJ, and $E_1 = 20$ mJ, $E_2 = 100$ mJ. At 2.76×10^7 Pa, the greatest intensity peak exists when ΔT has its smallest value (50 ns) (Fig. 4). The E_1 and E_2 that gave the greatest intensity were both in the range of 60–140 mJ. At a solution pressure of 1.38×10^7 Pa, the optimal ΔT was intermediate between

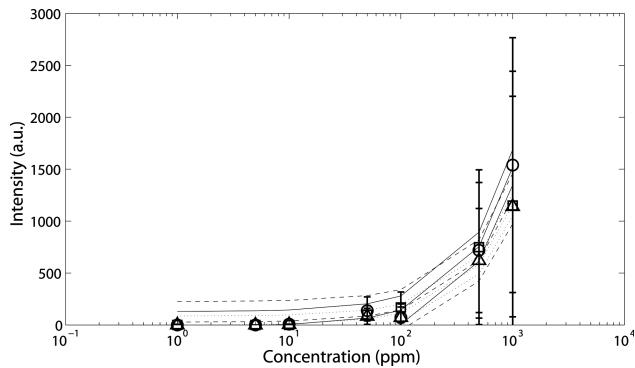


Fig. 13. Calibration curves calculated by a linear least squares fit of the concentration data and their 95% confidence limits on the coefficients for the Ca (I) 422 nm peak: \circ , solid line = 1×10^5 Pa, \square , dashed line = 1.38×10^7 Pa; Δ , dotted line = 2.76×10^7 Pa ($E_1 = 100$ mJ, $E_2 = 100$ mJ, $t_d = 50$ ns, and $\Delta T = 50$ ns).

that for 1×10^5 and 2.76×10^7 Pa (Fig. 3). At 2.76×10^7 Pa, a very intense peak was obtained for the condition $E_1 = 60$ mJ, $E_2 = 60$ mJ, $t_d = 50$ ns, and $\Delta T = 50$ ns. Therefore, a calibration curve was constructed using this condition as shown in Fig. 5. From this calibration curve and from the examination of spectra (Fig. 6), it is clear that Mg (I) is only detectable to about 5000 ppm.

B. Potassium

The results of the optimization studies for the 769.9 nm K (I) peak are shown in Figs. 7 and 8 for the atmospheric and high pressure (2.76×10^7 Pa) conditions. Potassium was detectable over an unusually wide range of conditions. Potassium has the lowest ionization energy (4.31 eV) of the elements that were studied, which contributes to ease of detection. In particular, a wide range of ΔT values were suitable at all pressures. At 1×10^5 and 1.38×10^7 Pa, the use of two high energy pulses resulted in the greatest peak intensity. At the highest pressure condition (2.76×10^7 Pa), a lower energy

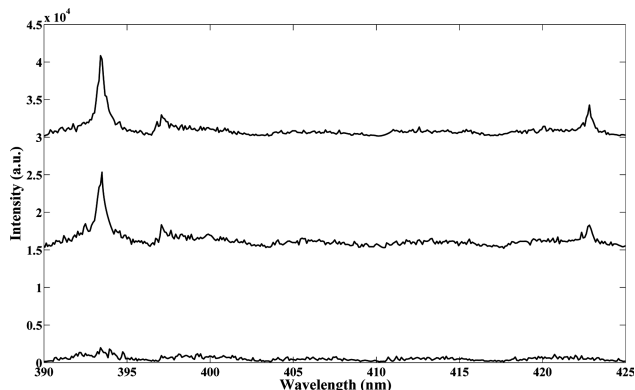


Fig. 14. Spectra of calcium (393 nm Ca (II), 396 nm Ca (II), and 422 nm Ca (I) peaks) at 2.76×10^7 Pa. Concentrations of spectra from bottom to top are 100 ppm, 500 ppm, and 1000 ppm ($E_1 = 100$ mJ, $E_2 = 100$ mJ, $t_d = 50$ ns, and $\Delta T = 50$ ns). For clarity, the spectra have been offset from each other by 15,000 a.u.

pulse followed by a higher energy pulse was advantageous. To construct a calibration curve, the conditions $E_1 = 100$ mJ, $E_2 = 140$ mJ, $t_d = 1000$ ns, and $\Delta T = 50$ ns were selected. The calibration curve and spectra of the calibration curve data (Fig. 9) reveal that K (I) is detectable to 500 ppm.

C. Calcium

The results for atmospheric pressure and the high pressure condition (2.76×10^7 Pa) for the 422 nm Ca (I) peak are shown in Figs. 10–12. At 1×10^5 Pa, the greatest intensity peak was detected when a long ΔT (500–5000 ns) with a low first energy pulse (typically 20 mJ) followed by a higher energy pulse (60–140 mJ). At both 1.38×10^7 and 2.76×10^7 Pa, the greatest intensity peak was observed for two high energy pulses (typically 100–140 mJ) separated by 50 ns. As a result, the conditions selected for the calibration curve were $E_1 = 100$ mJ, $E_2 = 100$ mJ, $t_d = 50$ ns, and $\Delta T = 50$ ns. The calcium calibration curve for the 422 nm Ca (I) peak reveals that the limit of detection for calcium using the conditions selected is 500 ppm (Fig. 13). This is also evident from looking at spectra under these conditions (Fig. 14).

D. Manganese

The optimization study results for the 403 nm Mn (I) peak are shown in Figs. 15 and 16. Although a Mn (I) triplet exists at 403 nm, peak broadening in liquids causes it to be unresolvable, and hence a single 403 nm peak is used for this study. At 1×10^5 Pa, a low first energy pulse (20 mJ) followed by a higher second energy pulse (60–140 mJ) with a long interpulse delay time (5000 ns) gave the greatest peak intensity (Fig. 15). When solution pressure was increased, the need for a significantly shorter ΔT was evident (Fig. 16). At the highest pressure condition, two high energy pulses gave the most intense peak (Fig. 16). Using a low second energy pulse (20 mJ) was not beneficial for this pressure condition. At the intermediate pressure (1.38×10^7 Pa) several parameter combinations can be used. Either a low energy first pulse (20 mJ) followed by a higher energy pulse (60–140 mJ) or two higher energy pulses (60–140 mJ) were suitable, and hence this is a transition pressure. For Mn (I), the conditions that were selected for the calibration curve were $E_1 = 100$ mJ, $E_2 = 60$ mJ, $t_d = 50$ ns, $\Delta T = 50$ ns. From both the calibration curve and the resulting spectra (Fig. 17), the limit of detection was 1000 ppm.

E. Sodium

The 588.995 nm Na (I) peak from the sodium doublet was used for optimization studies, and the results from two pressures are shown in Figs. 18 and 19. The highest intensity at 1×10^5 Pa was recorded when a low energy pulse was followed by a high energy pulse and a long ΔT was used (Fig. 18). For example, the greatest intensity was recorded for $E_1 = 20$ mJ, $E_2 = 140$ mJ, and $\Delta T = 5000$ ns. At

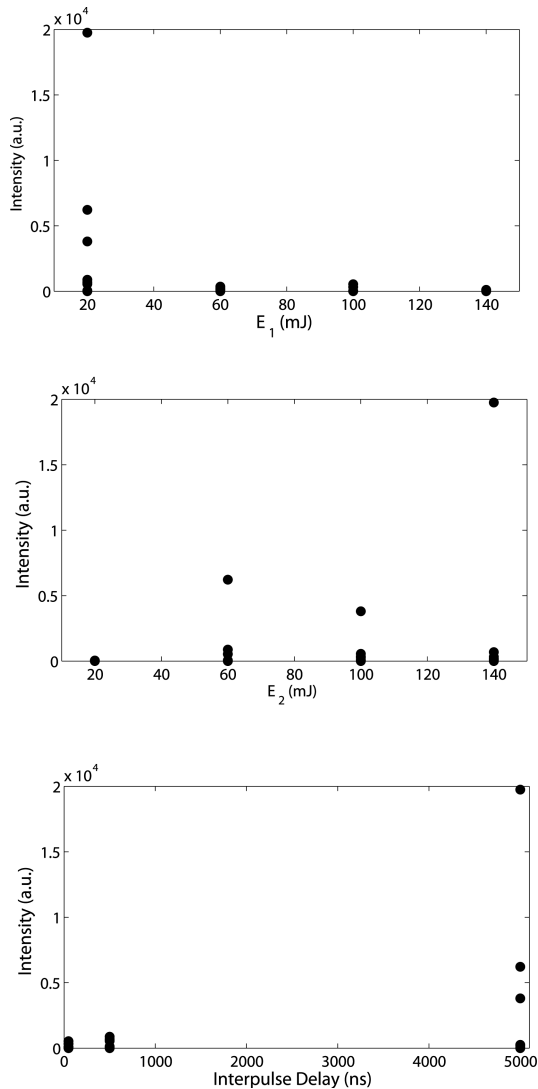


Fig. 15. Mn (I) (403 nm peak) optimization at 1×10^5 Pa. Each dot represents the peak intensity measured at one condition.

1.38×10^7 Pa, the greatest intensity peaks were recorded when two high energy pulses (60–140 mJ) were fired in rapid succession in either order and separated by 50 ns. Since ΔT is very small, these conditions approximate single pulse operation with a very high energy pulse. At 2.76×10^7 Pa, the greatest intensity peak again exists when two high energy pulses (60 and 140 mJ) are rapidly fired in either order separated by 50 ns (Fig. 19). The lowest intensity peaks were recorded at all pressures when the second energy pulse was 20 mJ, suggesting that the second pulse must be of sufficient irradiance to excite or reexcite plasma emission. The sodium calibration curve was therefore made at $E_1 = 60$ mJ, $E_2 = 140$ mJ, $\Delta T = 50$ ns, and $t_d = 50$ ns (see Fig. 20). Spectra at the high pressure (2.76×10^7 Pa) condition clearly indicate the limit of detection of 50 ppm (Fig. 21).

The limit of detection for sodium, as well as the other analytes reported here, is much higher than

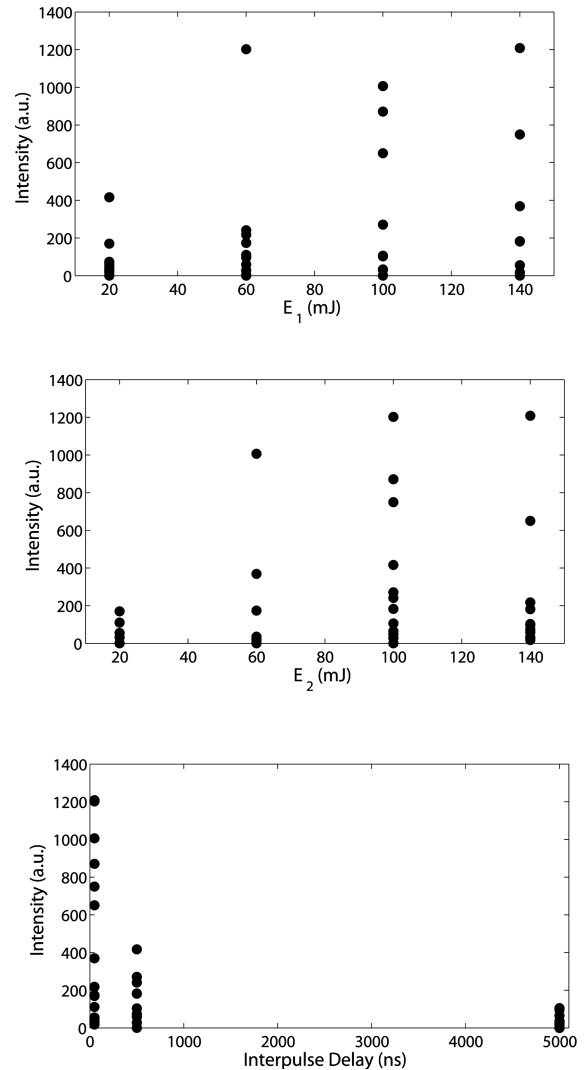


Fig. 16. Mn (I) (403 nm peak) optimization at 2.76×10^7 Pa. Each dot represents the peak intensity measured at one condition.

expected when compared to earlier studies [12,14]. In an effort to determine if the low optical throughput ($f/10$) Echelle spectrometer is the limiting factor, an additional calibration curve was completed at 1×10^5 Pa using optimal atmospheric pressure parameters. Lawrence-Snyder *et al.* reported the optimal ΔT for Na to be approximately 20 and 50 μs using a Chromex Czerny–Turner spectrometer ($f/4$) coupled to an ICCD camera at 3.4×10^6 Pa using $E_1 = 7$ mJ, $E_2 = 48$ mJ, and $t_d = 1$ μs [16]. In the present work, a low first energy pulse (20 mJ) followed by a high energy second pulse (140 mJ) was selected, and the corresponding optimal ΔT was determined. This ΔT was then used to create a calibration curve. To determine the optimal ΔT at atmospheric pressure, the peak intensity was measured at 1 μs , then at 5 μs , then at 5 μs intervals until a maximum ΔT of 170 μs . Figure 22 details the effect of ΔT on the intensity on the 588.995 nm Na (I) peak. The intensity is fairly uniform when ΔT is between 10 and 140 μs . After 140 μs , the intensity drops off. This plot

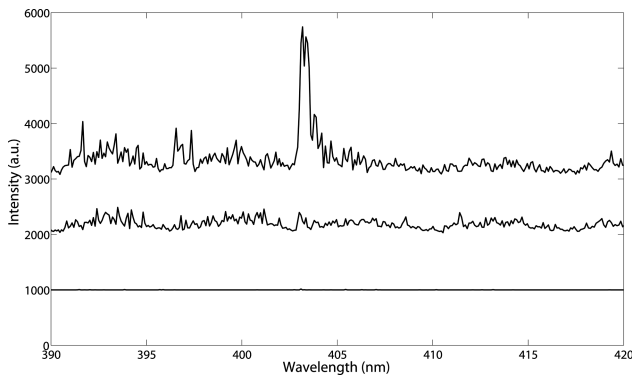


Fig. 17. Spectra of the Mn (I) peak (403 nm) at 2.76×10^7 Pa. Concentrations from bottom to top are 100 ppm, 500 ppm, and 1000 ppm ($E_1 = 100$ mJ, $E_2 = 60$ mJ, $t_d = 50$ ns, and $\Delta T = 50$ ns). For clarity, the spectra have been offset from each other by 1000 a.u.

supports the validity of selecting ΔT between 1 and 140 μ s; therefore, we select 70 μ s to construct a calibration curve. Comparing this time scale to that described by Lawrence-Snyder *et al.* [16], this result seems consistent due to our use of a significantly higher second energy pulse. Using the optimal condition with a long interpulse delay time, the detection limit is again only 50 ppm (Fig. 23), suggesting that the Echelle spectrometer is the limiting detection factor in these experiments.

4. Conclusions

DP-LIBS was used to detect five analytes in bulk aqueous solutions important in hydrothermal vent chemistry at pressures up to 2.76×10^7 Pa. The key DP parameters were optimized for each of the elements at three pressures (1×10^5 , 1.38×10^7 , and 2.76×10^7 Pa). The parameters needed for detection were found to be both element and pressure dependent. The use of an optimal set of parameters is essential because the analytes are often not detectable outside of the set. Potassium and sodium were detectable over a wide range of conditions. For all elements, as solution pressure was increased, the use of a shorter interpulse delay was necessary, and at 2.76×10^7 Pa, an interpulse delay time of the order of 50 ns should be used. For all conditions studied, a short gate delay (usually ≤ 100 ns) was required. The need for a short gate delay using both SP [19] and DP-LIBS for bulk liquid analysis suggests that in aqueous solutions, the plasma lifetime is very short, possibly lasting only of the order of 500 ns.

Using each of the optimally established conditions, calibration curves were constructed at three pressures (1×10^5 , 1.38×10^7 , and 2.76×10^7 Pa). From these, the limits of detection for the five analytes were found to be 5000 ppm Mg, 500 ppm K, 500 ppm Ca, 1000 ppm Mn, and 50 ppm Na using the current system setup. The limits of detection were the same for all three pressures tested. The main reason that LIBS researchers choose to use DP-LIBS instead of SP-LIBS is to achieve improved

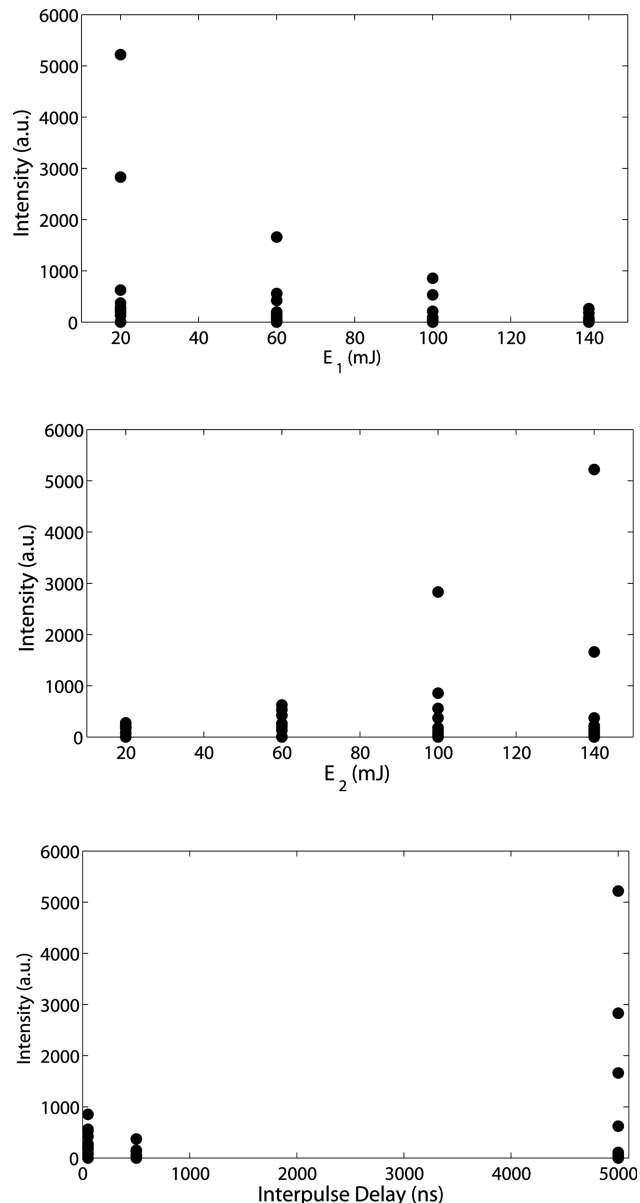


Fig. 18. Na (I) (588.995 nm) optimization at 1×10^5 Pa. Each dot represents the peak intensity measured at one condition.

sensitivity and improved signal. When optimization of conditions was completed using SP-LIBS and then subsequently calibration curves were made using the same system setup for the present work for Mn, Ca, and Na [19], the resulting limits of detection were found to be 500 ppm Mn, 500 ppm Ca, and 50 ppm Na. This suggests that the use of DP-LIBS in high pressure aqueous solutions may not be advantageous.

Lawrence-Snyder *et al.* reported no emission enhancement using DP-LIBS above 1×10^7 Pa [16]. De Giacomo *et al.* [24] emphasized the need for selecting an appropriate ΔT for underwater LIBS, stressing the need to optimize ΔT such that the second laser pulse causes the formation of a plasma in the laser-induced bubble, created by the first laser pulse, at its point of maximum expansion. It is the

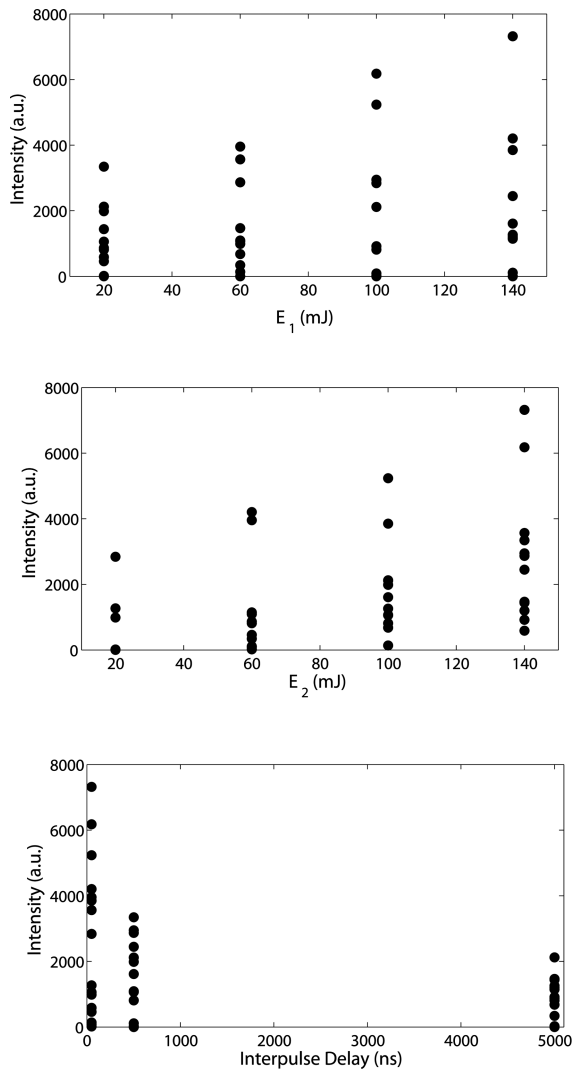


Fig. 19. Na (I) (588.995 nm) optimization at 2.76×10^7 Pa. Each dot represents the peak intensity measured at one condition.

orized that the high pressure aqueous environments used in our experiments may cause the bubble to collapse too rapidly to form a plasma. As a result, we

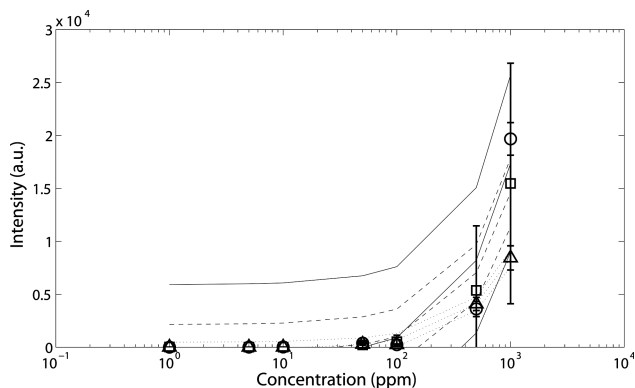


Fig. 20. Calibration curves calculated by a linear least squares fit of the concentration data and their 95% confidence limits on the coefficients for the Na (I) 588.995 nm peak. \circ , solid line = 1×10^5 Pa; \square , dashed line = 1.38×10^7 Pa; \triangle , dotted line = 2.76×10^7 Pa.

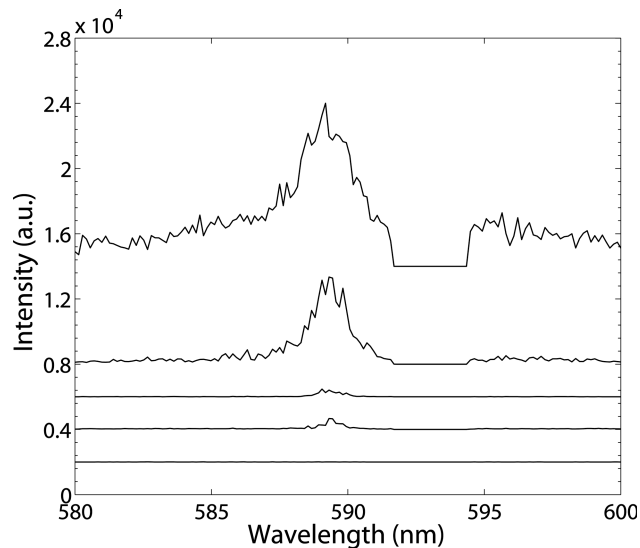


Fig. 21. Spectra of the Na (I) doublet peaks (588.995 nm and 589.6 nm) at 2.76×10^7 Pa. Concentrations from bottom to top are 10 ppm, 50 ppm, 100 ppm, 500 ppm, and 1000 ppm ($E_1 = 60$ mJ, $E_2 = 140$ mJ, $\Delta T = 50$ ns, and $t_d = 50$ ns). For clarity, the spectra have been offset from each other by 2000 a.u., except for the 1000 ppm spectrum which has been offset from the 500 ppm spectrum by 8000 a.u.

observe the highest intensity peaks when two laser pulses are fired close together, similar to a higher energy single pulse. Lawrence-Snyder *et al.* [31] suggest that at higher solution pressures (8×10^7 Pa), the bubble formed by the first laser pulse is confined by its surrounding pressure. As a result, the bubble never expands to the maximum volume that is observed at lower pressures so that emission enhancement does not occur.

Although the use of DP-LIBS proved less favorable than expected, it should be noted that one major contributing factor was the spectrometer used in these studies. The Echelle spectrometer has a very high resolution but a very low light throughput and poor sensitivity, with an f number of 10. In an effort to maximize the light throughput, it would be advisable to use a spectrometer with a smaller f number. As an example, the use of a spectrometer with an f number of 2 could possibly improve the

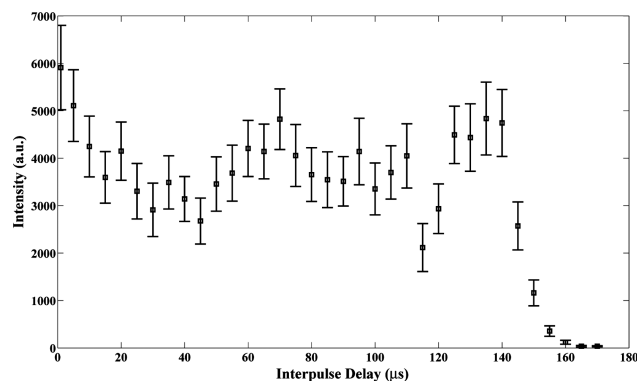


Fig. 22. Effect of interpulse delay on intensity on the 588 nm Na peak at 1×10^5 Pa (1000 ppm).

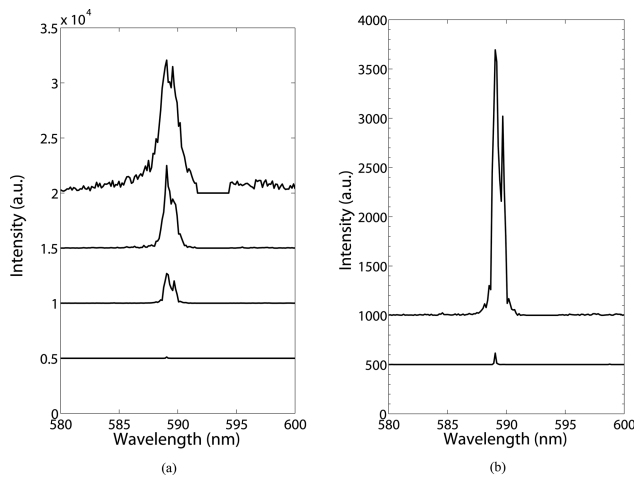


Fig. 23. Na (I) spectra at 1×10^5 Pa ($E_1 = 20$ mJ, $E_2 = 140$ mJ, and $t_d = 50$ ns).

throughput by a factor of 25, thus, improving the limits of detection. Furthermore, the use of a photomultiplier tube as the detector may improve detection limits for bulk liquids as demonstrated by Cremers *et al.*, who measured Na (I) (589.00 nm) to 0.014 ppm, K (I) (766.49 nm) to 1.2 ppm, Mg (II) (279.55 nm) to 100 ppm, and Ca (II) (393.37 nm) to 0.8 ppm at atmospheric pressure [12]. Further work is needed to maximize the light collection by changing system components for bulk aqueous solution experiments.

We acknowledge the National Science Foundation (NSF) for support of this research under grant OCE-0527927. Additional support was received from the Deep Ocean Exploration Institute and the Ocean Ventures Fund of the Woods Hole Oceanographic Institution.

References

1. R. S. Harmon, F. C. DeLucia, C. E. McManus, N. J. McMillan, T. F. Jenkins, M. E. Walsh, and A. Miziolek, "Laser-induced breakdown spectroscopy—an emerging chemical sensor technology for real-time field-portable, geochemical, mineralogical, and environmental applications," *Appl. Geochem.* **21**, 730–747 (2006).
2. Z. A. Arp, D. A. Cremers, R. C. Wiens, D. M. Wayne, B. Sallé, and S. Maurice, "Analysis of water ice and water ice/soil mixtures using laser-induced breakdown spectroscopy: application to Mars polar exploration.," *Appl. Spectrosc.* **58**, 897–909 (2004).
3. Z. A. Arp, D. A. Cremers, R. D. Harris, D. M. Oswald, G. R. Parker Jr., and D. M. Wayne, "Feasibility of generating a useful laser-induced breakdown spectroscopy plasma on rocks at high pressure: preliminary study for a Venus mission," *Spectrochim. Acta Part B* **59**, 987–999 (2004).
4. G. B. Courrèges-Lacoste, B. Ahlers, and F. R. Pérez, "Combined Raman spectrometer/laser-induced breakdown spectrometer for the next ESA mission to Mars," *Spectrochim. Acta Part A* **68**, 1023–1028 (2007).
5. R. Brennetot, J. L. Lacour, E. Vors, A. Rivoallan, D. Vailhen, and S. Maurice, "Mars analysis by laser-induced breakdown spectroscopy (MALIS): influence of Mars atmosphere on plasma emission and study of factors influencing plasma emission

with the use of Doehlert designs," *Appl. Spectrosc.* **57**, 744–752 (2003).

6. A. Knight, N. Scherbarth, D. Cremers, and M. Ferris, "Characterization of laser-induced breakdown spectroscopy (LIBS) for application to space exploration.," *Appl. Spectrosc.* **54**, 331–340 (2000).
7. B. Sallé, J.-L. Lacour, P. Mauchien, P. Fichet, S. Maurice, and G. Manhes, "Comparative study of different methodologies for quantitative rock analysis by laser-induced breakdown spectroscopy in a simulated Martian atmosphere," *Spectrochim. Acta Part B* **61**, 301–313 (2006).
8. C. R. German and K. L. Von Damm, "Hydrothermal processes," in *Treatise on Geochemistry*, H. Elderfield, H. D. Holland, and K. K. Turekian, eds. (Elsevier, 2003), Vol. 6, pp. 181–222.
9. J. H. Trefry, D. B. Butterfield, S. Metz, G. J. Massoth, R. P. Trocine, and R. A. Feely, "Trace metals in hydrothermal solutions from Cleft segment on the southern Juan de Fuca Ridge," *J. Geophys. Res.* **99**, 4925–4935 (1994).
10. K. L. Von Damm, "Controls on the chemistry and temporal variability of seafloor hydrothermal fluids," in *Seafloor Hydrothermal Systems: Physical, Chemical, Biological, and Geological Interactions*, Geophysical Monograph No. 91, S. Humphris, L. Mullineaux, R. Zierenberg, and R. Thomson, eds. (American Geophysical Union, 1995), pp. 222–247.
11. K. L. Von Damm, "Chemistry of hydrothermal vent fluids from 9°–10°N, East Pacific Rise: 'Time zero,' the immediate post-eruptive period," *J. Geophys. Res.* **105**, 11203–11222 (2000).
12. D. A. Cremers, L. J. Radziemski, and T. R. Loree, "Spectrochemical analysis of liquids using the laser spark," *Appl. Spectrosc.* **38**, 721–729 (1984).
13. R. Knopp, F. J. Scherbaum, and J. I. Kim, "Laser induced breakdown spectroscopy (LIBS) as an analytical tool for the detection of metal ions in aqueous solutions," *Anal. Bioanal. Chem.* **355**, 16–20 (1996).
14. W. Pearman, J. Scaffidi, and S. M. Angel, "Dual-pulse laser-induced breakdown spectroscopy in bulk aqueous solution with an orthogonal beam geometry," *Appl. Opt.* **42**, 6085–6093 (2003).
15. A. P. M. Michel, M. Lawrence-Snyder, S. M. Angel, and A. D. Chave, "Laser-induced breakdown spectroscopy of bulk aqueous solutions at oceanic pressures: evaluation of key measurement parameters," *Appl. Opt.* **46**, 2507–2515 (2007).
16. M. Lawrence-Snyder, J. Scaffidi, S. M. Angel, A. P. M. Michel, and A. D. Chave, "Sequential-pulse laser-induced breakdown spectroscopy of high-pressure bulk aqueous solutions," *Appl. Spectrosc.* **61**, 171–176 (2007).
17. M. Lawrence-Snyder, J. Scaffidi, S. M. Angel, A. P. M. Michel, and A. D. Chave, "Laser-induced breakdown spectroscopy of high-pressure bulk aqueous solutions," *Appl. Spectrosc.* **60**, 786–790 (2006).
18. A. De Giacomo, M. Dell'Aglio, F. Colao, R. Fantoni, and V. Lazić, "Double-pulse LIBS in bulk water and on submerged bronze samples," *Appl. Surf. Sci.* **247**, 157–162 (2005).
19. A. P. M. Michel and A. D. Chave, "Single pulse laser-induced breakdown spectroscopy of bulk aqueous solutions at oceanic pressures: interrelationship of gate delay and pulse energy," *Appl. Opt.* **47**, G122–G130 (2008).
20. A. E. Pichahchy, D. A. Cremers, and M. J. Ferris, "Elemental analysis of metals under water using laser-induced breakdown spectroscopy," *Spectrochimica Acta Part B* **52**, 25–39 (1997).
21. C. Haisch, J. Liermann, U. Panne, and R. Niessner, "Characterization of colloidal particles by laser-induced plasma spectroscopy (LIPS)," *Anal. Chim. Acta* **346**, 23–25 (1997).

22. P. K. Kennedy, D. X. Hammer, and B. A. Rockwell, "Laser-induced breakdown in aqueous media," *Prog. Quantum Electron.* **21**, 155–248 (1997).
23. A. De Giacomo, M. Dell'Aglio, and O. De Pascale, "Single pulse-laser induced breakdown spectroscopy in aqueous solution," *Appl. Phys. A* **79**, 1035–1038 (2004).
24. A. De Giacomo, M. Dell'Aglio, O. De Pascale, and M. Capitelli, "From single pulse to double pulse ns-laser induced breakdown spectroscopy under water: elemental analysis of aqueous solutions and submerged solid samples," *Spectrochim. Acta Part B* **62**, 721–738 (2007).
25. A. Casavola, A. De Giacomo, M. Dell'Aglio, F. Taccogna, G. Colonna, O. De Pascale, and S. Longo, "Experimental investigation and modelling of double pulse laser induced plasma spectroscopy under water," *Spectrochim. Acta Part B* **60**, 975–985 (2005).
26. A. De Giacomo, M. Dell'Aglio, F. Colao, and R. Fantoni, "Double pulse laser produced plasma on metallic target in seawater: basic aspects and analytical approach," *Spectrochim. Acta B* **59**, 1431–1438 (2004).
27. S. Koch, R. Court, W. Garen, W. Neu, and R. Reuter, "Detection of manganese in solution in cavitation bubbles using laser induced breakdown spectroscopy," *Spectrochim. Acta Part B* **60**, 1230–1235 (2005).
28. V. Lazic, F. Colao, R. Fantoni, and V. Spizzichino, "Laser-induced breakdown spectroscopy in water: improvement of the detection threshold by signal processing," *Spectrochim. Acta Part B* **60**, 1002–1013 (2005).
29. R. Noll, "Terms and notations for laser-induced breakdown spectroscopy," *Anal. Bioanal. Chem.* **385**, 214–218 (2006).
30. A. P. M. Michel and A. D. Chave, "Analysis of laser-induced breakdown spectroscopy spectra: the case for extreme value statistics," *Spectrochim. Acta Part B* **62**, 1370–1378 (2007).
31. M. Lawrence-Snyder, J. P. Scaffidi, W. F. Pearman, and S. M. Angel, "Dependence of emission intensity on bubble dynamics in dual-pulse laser-induced breakdown spectroscopy of high-pressure bulk aqueous solutions," submitted to *Appl. Spectrosc.*